Investigation on Fatigue Behavior of Alloys by Various Approaches

by

Siying Liu

A Thesis Presented in Partial Fulfillment
of the Requirements for the Degree
Master of Science

Approved July 2018 by the
Graduate Supervisory Committee:

Yongming Liu, Chair
Yang Jiao
Qiong Nian

ARIZONA STATE UNIVERSITY

August 2018

ABSTRACT

Fatigue is a degradation process of materials that would lead to failure when materials are subjected to cyclic loadings. During past centuries, various of approaches have been proposed and utilized to help researchers understand the underlying theories of fatigue behavior of materials, as well as design engineering structures so that catastrophic disasters that arise from fatigue failure could be avoided. The stress-life approach is the most classical way that academia applies to analyze fatigue data, which correlates the fatigue lifetime with stress amplitudes during cyclic loadings. Fracture mechanics approach is another well-established way, by which people regard the cyclic stress intensity factor as the driving force during fatigue crack nucleation and propagation, and numerous models (such as the well-known Paris' law) are developed by researchers.

The significant drawback of currently widely-used fatigue analysis approaches, nevertheless, is that they are all cycle-based, limiting researchers from digging into sub-cycle regime and acquiring real-time fatigue behavior data. The missing of such data further impedes academia from validating hypotheses that are related to real-time observations of fatigue crack nucleation and growth, thus the existence of various phenomena, such as crack closure, remains controversial.

In this thesis, both classical stress-life approach and fracture-mechanics-based approach are utilized to study the fatigue behavior of alloys. Distinctive material characterization instruments are harnessed to help collect and interpret key data during

fatigue crack growth. Specifically, an investigation on the sub-cycle fatigue crack growth behavior is enabled by in-situ SEM mechanical testing, and a non-uniform growth mechanism within one loading cycle is confirmed by direct observation as well as image interpretation. Predictions based on proposed experimental procedure and observations show good match with cycle-based data from references, which indicates the credibility of proposed methodology and model, as well as their capability of being applied to a wide range of materials.

DEDICATION

To my family

ACKNOWLEDGMENTS

I would like to express my sincere gratitude to my faculty advisor Prof. Yongming Liu, an erudite scholar, for his support upon my master's study and research. I couldn't have completed my master's thesis without his guidance and help.

I also gratefully appreciate my thesis defense committee members: Prof. Yang Jiao and Prof. Qiong Nian, and their conducive advice upon my research as well as the revision of my thesis.

Many thanks to my group members that offered tremendous help and suggestions during my academic life here at Arizona State University. Special thanks to my pal Zhongyong Wang, who sets up a high standard for me and shows me what an eminent PhD student with infinite potential as well as devotion should be like, I appreciate his selfless help upon on both my research and personal life. Also, I appreciate Alyssa Nazareno for her dedicated work on part of experimental research contained in this thesis.

Thanks to my friends back in China, Xiaoyun Ye, Hongren 'puck' Lin, and Han Gao for helping me go through those hard times.

TABLE OF CONTENT

Page

LIST OF TABLES

Tables Page

LIST OF FIGURES

Figures Page

Figures Page

Figures Page

Chapter 1

INTRODUCTION

1.1 Overview

Fatigue is usually defined as a materials' and structural components' degradation process that would lead them to crack or fail when they are subjected to cyclic loadings. In the past years, researchers and engineers have been working on this topic to unveil its fundamental mechanisms and prevent catastrophic failures. Various research methodologies and theoretical models have been developed for this purpose. Most of the scientific approaches that people adopt can be categorized into two. Stress-life approach, which was originated from Wöhler's work, correlates materials' and components' lifetime with the cyclic stresses they are subjected to. The number of stress or strain cycles needed for fatigue failures in initially uncracked materials or components is tested and estimated under certain cyclic stress or strain amplitudes [1]. The estimated total lifetime contains two portions: number of cycles for a dominant crack nucleation, and number of cycles for such crack to propagate and eventually cause catastrophic fatigue failure. Extensive work has been done to address the contributions from mean stresses, geometries of the components, environmental and many other factors upon the total cyclic lifetime of metals, polymers, ceramics and many other materials.

The other classical approach, first proposed by Paris [2] during the 1960s, lies its theoretical fundamental on fracture mechanics. This model correlates the fatigue crack growth rate per cycle da / dN with the applied stress intensity factor range ΔK,

and has gained its dominant position in fatigue research. Based on the essential characteristics of fatigue, it is unassailable that researchers use cyclic quantities and parameters to account for fatigue behavior of materials and components, which is the essential principle of both stress-life approaches and Paris' law. Nevertheless, due to the limitations of cycle-based theories and models on fatigue as well as the unavailability of appropriate research instruments, it is hard to quantitatively study the fatigue crack growth behavior within each cycle, or to validate the existence of phenomena that have long been in argument, such as crack closure. To lay a theoretical basis for such research purposes, Zizi Lu and Yongming Liu [3] proposed a small-time-scale fatigue model whose methodology is fundamentally different from classical cycle-based fatigue models ($da\ /\ dN$) as it describes and predicts instant fatigue crack growth behavior ($da\ /\ dt$). With the help of high-resolution scanning electron microscopy and in-situ mechanical testing instruments, it becomes possible for researchers to investigate the sub-cycle behavior of fatigue crack growth for a variety of materials.

1.2 Structure of Thesis

The main body of this thesis consists of two major parts that are based on two distinctive research methodologies.

In chapter 2, a classical stress-life approach is applied to study the fatigue lifetime behavior of a certain bridge steel. The steel is sorted into two categories: one with a corrosion surface, i.e., the corrosion fatigue scenario, and the other pure mechanical fatigue as no surfaces is corroded. Morphological analysis is also included

with the help of various material characterization tools.

In chapter 3, an investigation on the instantaneous fatigue crack growth behavior of two types of alloys is carried out based on small-time-scale fatigue crack growth model. To achieve the real-time crack growth observation and measurements, an in-situ SEM fatigue testing technique is adopted by the combination between scanning electron microscopy as well as mechanical tensile testing system. The idea of this chapter is to further validate the accuracy and universality of the proposed model.

Chapter 2

INVESTIGATION ON FATIGUE BEHAVIOR OF A CERTAIN BRIDGE STEEL BY S-N APPROACH

2.1 Introduction

S-N approach is a widely acknowledged, phenomenological continuum approach that characterizes the total fatigue life time as a function of variables such as applied stress/strain range, mean stress and environment [1]. Here, S represents stress, and N stands for number of cycles to failure. Micromechanical processes and phenomena, such as fatigue damage evolution, crack nucleation, crack growth behavior, are embedded into a single, experimentally characterizable continuum formulation, which is the essential idea of S-N approach. An S-N curve, which is the statistical presentation of the above-mentioned approach, is also named as a Wöhler curve to honor the earliest effort by German engineer who first observed and studied the fatigue behavior of railroad car wheels back to 1860s.

One of the most important concepts addressed in S-N curve approach is 'endurance limit' (originated from Wöhler's work, now the terminology 'fatigue limit' is more spread and accepted, which will also be used in this thesis). Fatigue limit denotes an applied stress amplitude below which the material could survive infinitely without going through fatigue failures. S-N approach is especially useful and accurate when researchers are working on materials that serve under high-cycle fatigue, where the cyclic stress amplitudes are low, and almost only elastic deformation is involved.

Extensive work has been done by scientists and engineers to address materials'

fatigue properties by S-N curve approach. Materials show distinctive fatigue behavior that is related to their diverse structural and mechanical properties. Steels, for example, generally exhibit a fatigue limit, which stands for a stress level below which they would not fail under cyclic loadings. Non-ferrous metals and alloys, on the other hand, don't have such a typical fatigue limit. Cyclic stress amplitude for these materials would continue decreasing with the increase of number of cycles. In this case, a widely-accepted fatigue limit is defined as the stress level at which the material could survive with a minimum number of cycles equivalent to 10^7. Typical S-N curves for steels and non-ferrous metals can be seen in Figure 1.

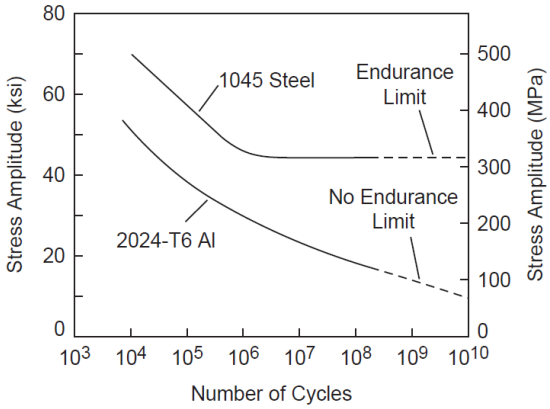

Figure 1 Typical S-N curves for steel and Aluminum alloy [4].

Things become more complicated and esoteric if we investigate the S-N responses or polymetric materials, as a special phenomenon called crazing is involved. For those polymers exhibiting crazing behavior, a flat plateau will arise in their S-N curves, whereas polymers without it would often demonstrate a S-N response similar to that of metals. Contributions from many other factors, such as morphological, thermal, mechanical and environmental effects are also involved in fatigue behavior of polymers, hence this topic would not be covered in detail as it's beyond the scope of

this thesis.

Due to the fact that the to-be-tested specimens are obtained from an abandoned bridge (which will be discussed in the following sections with detailed information), contributions from detrimental environment along with cyclic loading conditions must also be investigated. An external medium can be deleterious to materials and structures under cyclic loading and severely undermine their fatigue strength. As a consequence, it's imperative to constitute the environmental factors into fatigue theory and the term 'corrosion fatigue' is denoted to address such scenarios. Corrosion fatigue is dependent on a variety of factors, such as materials' structural, mechanical and metallurgical properties, cyclic loading conditions, material-environment interactions, and so on.

As for the fatigue life of materials, the main difference between corrosion fatigue and fatigue in inert environments is that there would be no fatigue limits for metals, i.e., metals undergoing corrosion fatigue would always fail if given enough time. A schematic comparison between S-N curves of pure fatigue and corrosion fatigue of steel is depicted in Figure 2. While there being no crack nucleation if applied stress is below fatigue limit in pure fatigue, damage caused by corrosion (corrosion pits, for example) would serve as stress concentration sites when corrosion is involved. Furthermore, as corrosion would always happen at the surfaces of components, corrosion fatigue cracks will always nucleate at the corroded surfaces (assuming no cavities or voids underneath the surfaces). As for the case of carbon steels, cracks would oftentimes nucleate at corrosion pits and contain corrosion products, propagate trans-granularly and present branching [5].

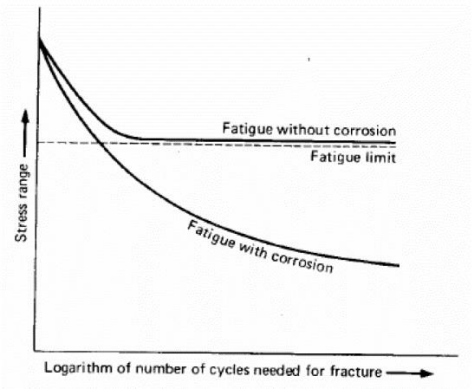

Figure 2 Schematic S-N curves for pure and corrosion fatigue behavior of steel [6].

2.2 Experimental Procedures

2.2.1 Specimen Design and Preparation

Material used to fabricate fatigue specimens was acquired from The Pearl Harbor Memorial Bridge (Q-bridge) in New Haven, which has been replaced as part of the $2-billion I-95 New Haven Harbor Crossing Corridor Improvement Program. After the demolition of the old bridge, steel obtained has been provided by The Connecticut Department of Transportation (CTDOT) for research purpose. Unfortunately, since the Q-bridged was designed and constructed back in the 1950s when the World War II was just over, missing of the historical documents leads to the ambiguity of standard used to instruct the project. It is not clear whether A7 buildings and Bridges standard in 1939 or A7 WPB Emergency Standards in 1942 was used, hence the exact properties of the given material cannot be determined besides the fact that it's steel.

Geometry of the fatigue specimens is shown in Figure 3. The design and fabrication follow ASTM E466-15: Standard Practice for Conducting Forced Controlled Constant Amplitude Axial Fatigue Tests of Metallic Materials. Specimens are sorted into two categories:1) with corrosion on one surface; 2) without corrosion on

both surfaces (corrosion surfaces are removed by machine sanding). A set of specimens without corrosion surfaces are used to establish the reference S-N curve indicating the pure fatigue scenario and compare with the S-N curve obtained for the case of corrosion fatigue. All to-be-tested specimens are measured and recorded individually to get accurate cross-sectional areas, and then labeled accordingly.

Photos of the corroded and uncorroded surfaces can be seen in Figure 4. The red rectangular region indicates the surface area for the optical profilometry which is utilized to acquire surface corrosion profiles. Rectangular region is located at which the fracture is predicted to happen based on the specimen geometry as well as the loading conditions.

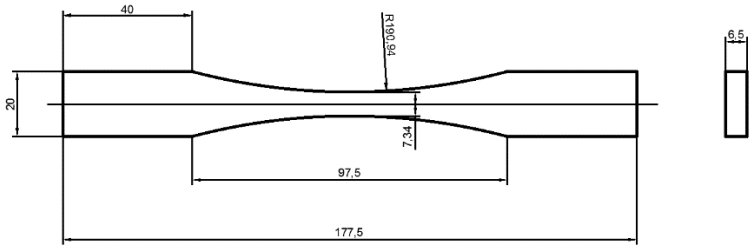

Figure 3 Geometry of the designed fatigue specimens.

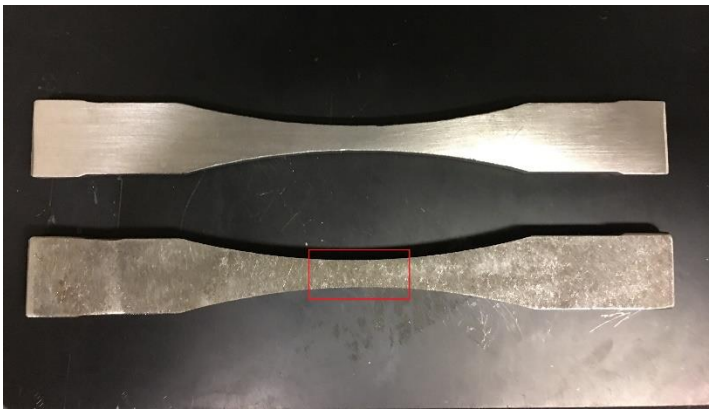

Figure 4 Corroded and clean surfaces, rectangular region indicates the surface area for optical profilometry.

2.2.2 Experimental Setup and Procedures

Before running the tests, specimens are observed by ZEISS EVO MA 10

Scanning Electron Microscope to get microscopic images of the corrosion surfaces. Optical profilometry of the corrosion surfaces are also obtained by a ZeScope Optical Profilometer from Eyring Materials Center at ASU.

Fabricated fatigue specimens are installed onto the MTS Landmark servohydraulic test system for fatigue test with constant amplitudes. The load cells of the test system have the dynamic/static force capacities of $100kN$ / $120kN$. After installation, grip pressures are tuned according to the grip pressure calculating equation for dynamic loadings provided by MTS manual so that sufficient grip pressures are guaranteed to keep the specimens properly held. Setup of the fabricated specimens on the MTS Landmark servohydraulic test system can be seen in Figure 5.

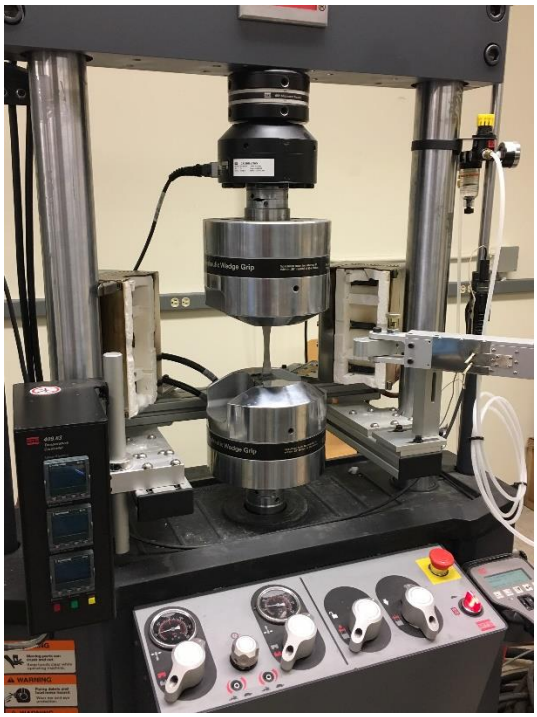

Figure 5 Fatigue specimen installed onto MTS servohydraulic test system.

All tests are implemented by force-control mode, with constant loading frequency of $10Hz$. A sinusoidal loading profile is adopted. Target setpoints and

amplitudes of applied forces are calculated based on the desired stress level as well as the cross-sectional areas respectively. Proper PID tuning and compensator are used to acquire accurate force gains. Force and displacement interlocks are setup to monitor test status and enable an automatic shutdown when the tests finish, i.e., the specimens completely break into two pieces. Real-time meters and cycle counter are used to monitor instantaneous axial force and displacement as well as record each specimen's N_f. All the above-mentioned settings are achieved by MTS Station Manager, which is a software controlling the test system. Software interfaces and the sinusoidal loading profile can be seen in Figure 6.

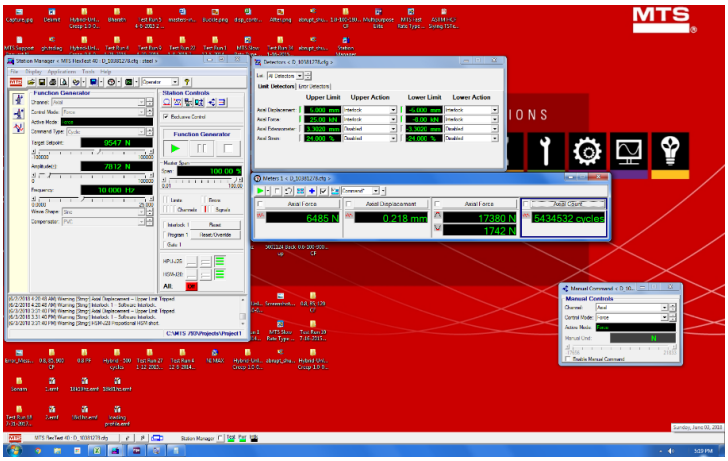

(a)

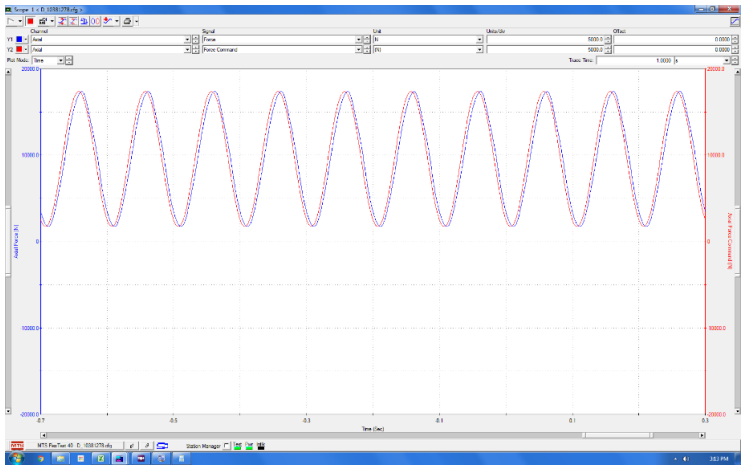

(b)

Figure 6 (a) MTS Station Manager interfaces and (b) sinusoidal loading profile.

Fractured specimens are altered by cutting to obtain small pieces (depicted in Figure 7) for SEM observations of the fracture surfaces. All the above-mentioned fabrication and alteration work is done by the Mechanical & Electrical Workshop at ASU.

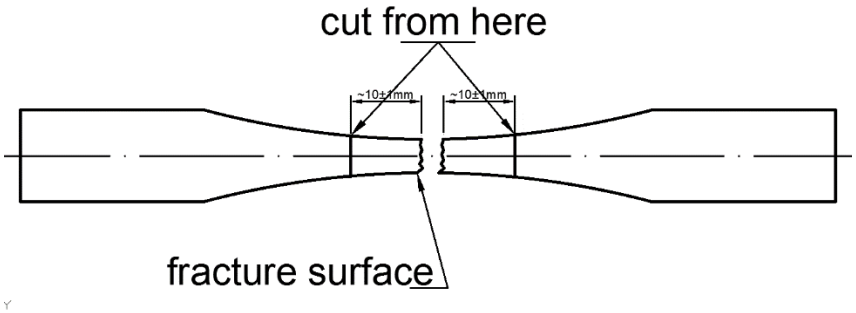

Figure 7 Small pieces cut from fractured specimens for SEM observations.

Once the overall S-N curves for both corroded and uncorroded specimens have been determined based on experimental data, two sets of to-be-tested specimens would be prepared for the following purpose:

(1) For the first set of specimens, an appropriate stress level will be selected, and these specimens would be tested subject to this stress level. In this way, fatigue lifetime and statistical behavior of the tested material can be examined and verified.

(2) Another set of specimens is prepared in order to test the effect of cumulative damage on the fatigue lifetime of the material. Palmgren-Miner rule is often used to address the cumulative damage during fatigue with variant loadings and amplitudes. Palmgren-Miner rule assumes that during cyclic loadings, the total lifetime of a material or component subjected to the loadings can be estimated by taking the sum of the percentage of lifetime consumed by each stress level, shown in Equation (1).

$$\sum_{j=1}^{j=k} \frac{n_j}{N_j} = 1 \tag{1}$$

2.3 Results and Discussions

2.3.1 Morphological Analysis

Based on the location of the bridge, the deleterious aqueous medium can be determined as combination of fresh water as well as sea water. In such noxious environment, the key ingredients are believed to be chlorides. Structural components (in this case, steel bridge girders) would be exposed to aqueous chloride environments where ambient salt aerosol contaminants result in a wetted surface under ambient humidity. Aqueous chloride environments are believed to be capable of inducing local corrosion damage, undermining the overall fatigue lifetime as well as enhancing the crack propagation rates[7]–[10].

SEM images of the corrosion surface at different magnifications are depicted in Figure 8. Figure 8 (a) shows an overall morphology of the corrosion surface. The surface is subjected to general corrosion, which means the corrosion process behaves uniformly over the entire surface. Such a process would cause an overall reduction in the component's thickness, and thus a shortened fatigue lifetime due to the increasement of stress amplitude. Variations in contrast stand for changes in the heights of the corrosion surface, which indicates the necessity of height profile of the corrosion surface by optical profilometry. What's more, the existence of surface corrosion is altering the surface roughness, which also plays a key role in a component's overall fatigue lifetime [11]. Majority of the black dots seen on the surface is corrosion pits with different depths and sizes. Figure 8 (b) and (c) both demonstrate zoomed-in images of corrosion at center and edges of the surface. The diameter of the pit in Figure 8 (b)

is about $125\mu m$. Specifically, the corrosion pit shown in Figure 8 (c) has a diameter of $276.4\mu m$, and the huge difference in depths of the fields between the bottom of the pit and its surrounding area also speaks for the large depth of the pit. Such a tremendous size, along with the fact that it's located at the edge of the corrosion surface at which the applied stress concentrates, indicates the high probability of this pit serving as the initial crack nucleation site during the fatigue test.

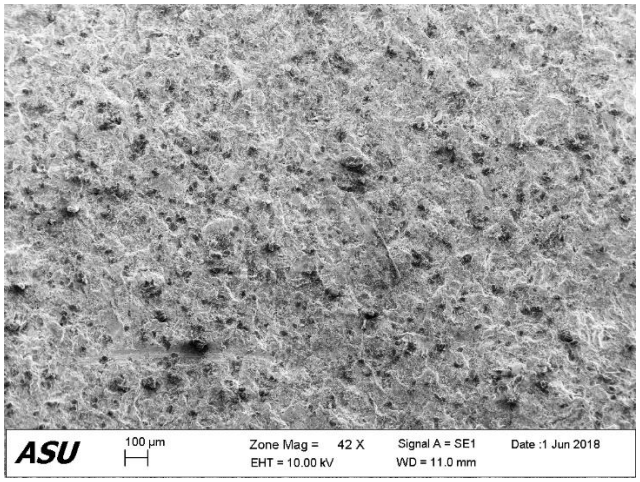

(a)

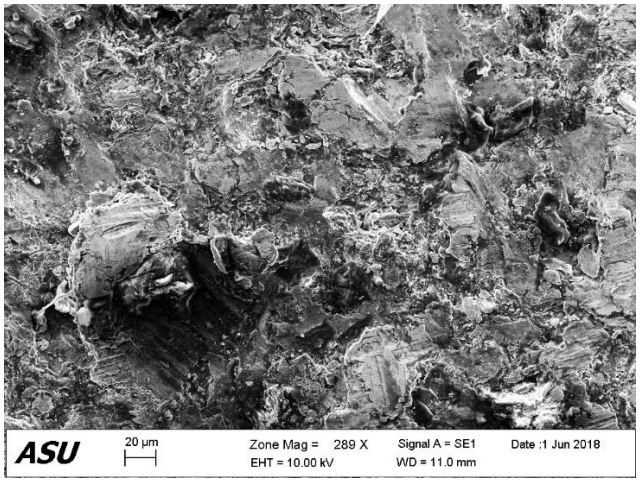

(b)

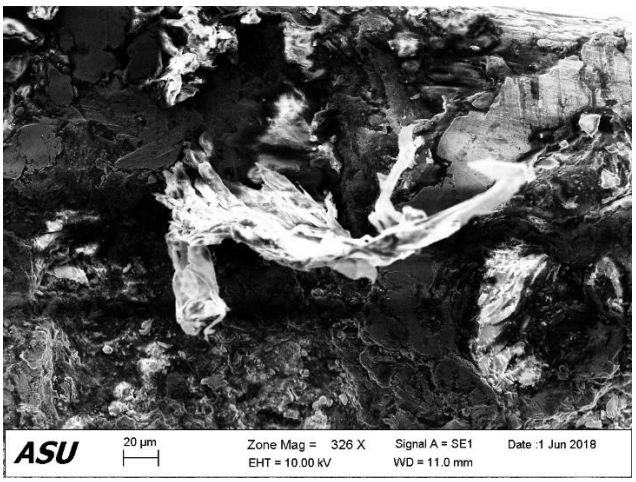

(c)

Figure 8 SEM images of the corrosion surface at various magnifications: (a) overall morphology of the corrosion surface; (b) zoomed-in image indicating the corrosion pit and (c) a particularly severe corrosion pit predicted to be crack nucleation site.

Optical profilometry is also used to detect the surface morphology and reconstruct the corrosion surface height profile with a 3D contour map. A reconstructed 3D map of the corrosion surface with the rectangular region (as shown in Figure 4) is demonstrated in Figure 9. The length bar indicates range of the depths, with color varying from yellow to red with respect to the changing height. Peaks appeared on the contour stand for signal noises. It can be seen from the image that the maximum difference in height between the highest and lowest regions is about $100\mu m$, which provides a quantitative view of the corrosion surface. One can note that the regions with larger depths (red-colored areas), i.e., regions undergoing more severe corrosion damage, mainly lie on the edge of the corrosion surface. This is of great importance for predicting possible crack nucleation sites during the fatigue test since cracks tend to nucleate in regions with worse corrosion damage due to their weakened local strength. The black circle highlights a local valley on the corrosion surface with a huge height contrast, leading to an even higher chance for the failure to start here, as the valley can

already be regarded as a local crack. Furthermore, since the circled area lie at the very edge of the corrosion surface, the stress concentration of this area is much higher than those areas lie within the center of the surface. The coupling effect of surface corrosion damage and loading conditions can be concrete proof of crack nucleation site predictions.

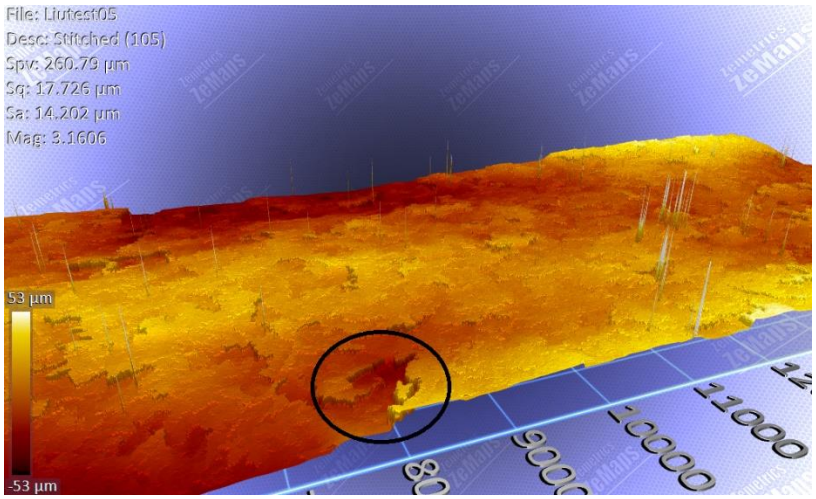

Figure 9 A reconstructed 3D map of corrosion surface, with the black circle indicating a sharp valley.

A photo of fractured fatigue specimen can be seen in Figure 10, the bending surface close to the fractured region clearly indicates a tensile failure.

Figure 10 Fractured fatigue specimen.

Fracture surface morphology of a fractured specimen with corrosion is acquired by SEM observation, as is depicted in Figure 11. Figure 11 (a) shows the overall

morphology of the fatigue fracture surface at low magnifications. The red solid line at bottom indicates the longitudinal corrosion surface. The fracture surface is divided into two distinctive regions, which corresponds to two phases before the specimen completely fails. The yellow dash line demonstrates the boundary between the two above-mentioned phases, with red solid arrows indicating the crack propagation direction. Three individual regions marked by 1, 2 and 3 are discussed in detail. Region 1 shows the crack initiation region, and a main crack at the very bottom of region 1, i.e., on the edge of the longitudinal corrosion surface, is captured and depicted in Figure 11 (b). The crack has a width of over $60\mu m$, enabling the local stress concentration and thus the crack starts to grow and propagate. The white-color area represents the corrosion product, which penetrates deeply through the surface, causing weakened local strength. Two distinctive phases are observed in region 2 and 3 and are shown in Figure 11 (c). Region 2 indicates the relatively slow fatigue crack propagation at the early stage, the surface morphology is relatively smooth and flat, with stripes whose orientation is consistent with the propagation direction. It must be noted that benchmarks are not seen on this fracture surface morphology, which is attributed to metallurgic factors. When the crack front pushes to the yellow dash line, the crack length reaches a critical level under the applied stress, thus catastrophic rupture happens which leads to the complete failure of the specimen. Region 3 is characterized by rough surface along with the presence of dimples, which is commonly seen in rupture of steel undergoing high tensile stresses.

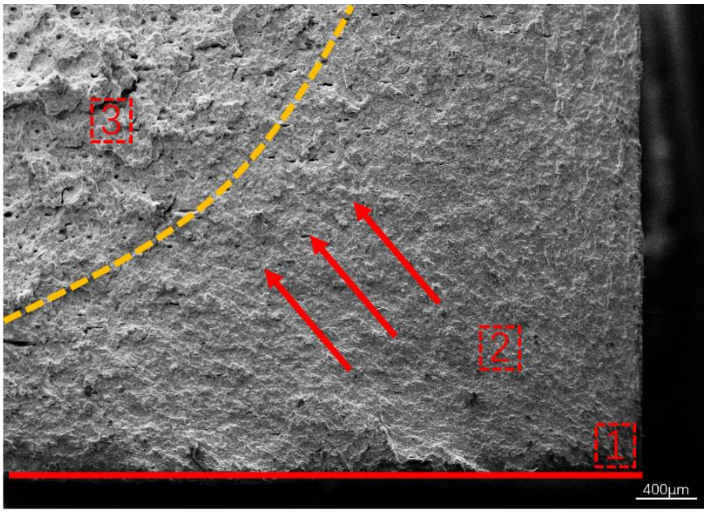

(a)

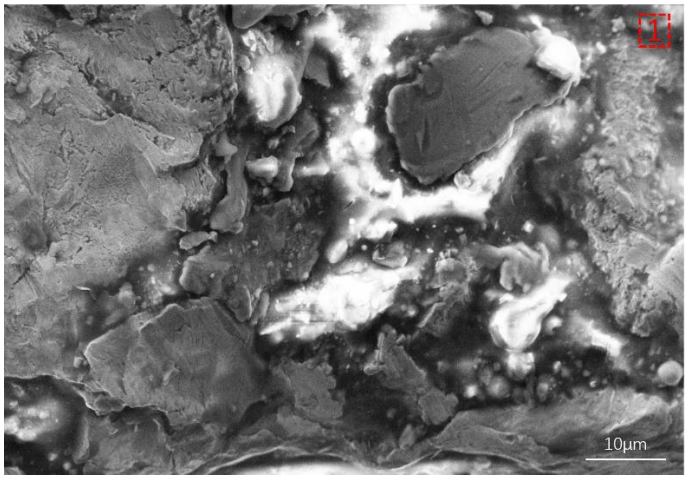

(b)

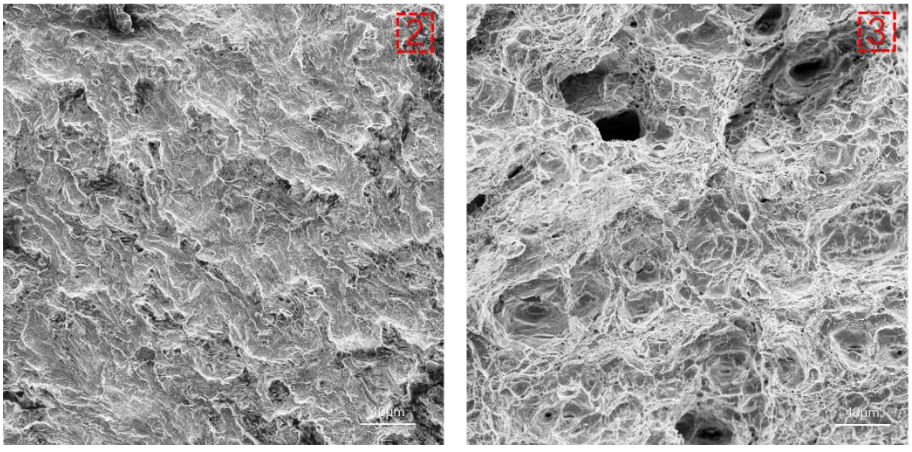

(c)

Figure 11 SEM images of the fatigue fracture surface: (a) overall morphology of the fracture surface; (b) zoomed-in image of the crack initiation site and (c) detailed morphology of the region 2 and 3, indicating two different phases of before final rupture.

Direct observations confirm the significant fact that for all fatigue specimens with corrosion surfaces, the cracks start at the edge of the corrosion surface within the rectangular region shown in Figure 4. For moderate stress levels, the cracks start at one edge and propagate until the specimens fail, whereas when the applied stress is sufficiently high, cracks initiate at both corners. These direct observations are consistent with the morphological analysis by both SEM and optical profilometer, and such results lead to the conclusion that it is possible to predict crack initiation sites for specimens with designed geometry undergoing fatigue corrosion.

2.3.2 S-N Curve and Data Analysis

Plots illustrating the S-N curves for both specimens with corrosion and uncorroded specimens can be seen in Figure 12. Here the stress range, i.e. $S = \sigma_{max} - \sigma_{min}$, is denoted as S. The overall trends of both curves show decent match with the schematic curves shown in Figure 1. At high stress levels, curves of both types of specimens show good match and have similar lifetimes, indicating the fact that when applied stresses are high, stresses become the overwhelming factor over the existence of corrosion surface and corrosion pits. The curve that stands for the uncorroded specimens begin to deviate from the other curve when applied stresses reduced. This is attributed to the fact that the existence of surface corrosion and corrosion pits serve as natural and effective crack nucleation sites that could significantly reduce or even eliminate the initiation portion of fatigue lifetime, whereas for the uncorroded specimens, ideally only stress concentration on the surface discontinuity (which in this case is corner of the specimen) contributes to the crack initiation due to the formation

of persistent slip bands. When the applied stress reduces to $351MPa$, the uncorroded specimen survives over 2 million cycles without failure, which can be regarded as the fatigue limit. Whereas the tested specimen with corrosion surfaces failed at 427650 and 682968 cycles when subjected to stress ranges of $351MPa$ and $346.5MPa$, respectively.

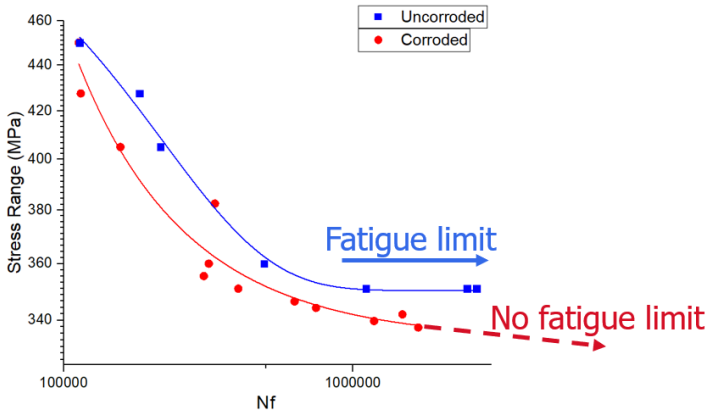

Figure 12 S-N curves of the corroded and uncorroded specimens.

The gap between two curves is not drastically different, which can be possibly explained by the following:

(1) The damage induced by the surface corrosion is not large enough to cause a huge reduction in the time needed for crack nucleation and hence, a reduction in total lifetime.

(2) Tested specimens had been in service for decades before they were collected from the abandoned bridge and refabricated for experimental purpose. Hence the portion of crack nucleation among total lifetime, which often goes up to 90%, had been significantly shortened during their service.

(3) Due to the limited number of tested specimens. It's well-known that during fatigue tests commercial materials subjected to identical stress amplitude show

noticeable uncertainties in total lifetime, and ideally if a sufficiently large number of specimens is tested, a Gaussian or normal distribution is expected at each stress level. Here we only have limited available specimens and thus the S-N curved fitted out of these data points may not be accurate enough.

Another 2 sets of specimens are tested at a constant stress range of $360MPa$ as well as $405MPa$ to verify their fatigue lifetime distributions. Geometries, maximum applied forces and numbers of cycles to failure of the tested specimens can be seen in Table 1 and Table 2.

Table 1 Fatigue lifetime data for 5 samples at stress range $360MPa$.

Thickness (mm)	Width (mm)	Area (mm^2)	Max force (N)	# of cycles
6.20	7.35	45.57	18228	473928
6.22	7.33	45.59	18237.4	292426
6.20	7.33	45.45	18178.4	492134
6.23	7.33	45.67	18266.4	422208
6.18	7.33	45.30	18119.8	426672

Table 2 Fatigue lifetime data for 5 samples at stress range $405MPa$.

Thickness (mm)	Width (mm)	Area (mm^2)	Max force (N)	# of cycles
6.16	7.36	45.34	20401.9	230736
6.26	7.35	46.01	20705.0	249504
5.97	7.36	43.94	19772.6	217442
5.85	7.36	43.06	19375.2	176368
6.21	7.38	45.83	20623.4	224102

For the 2 sets of specimens tested at stress range $360MPa$ and $405MPa$, average number of cycles to failure $\bar{N}$, standard deviations of numbers of cycles to failure σ are $\bar{N}_{360} = 421473.6$, $\sigma_{360} = 69893.06$, $\bar{N}_{405} = 219630.4$, $\sigma_{360} = 24133.74$,respectively. It can be clearly seen that the overall distributions of both sets are not greatly scattered, which indicates the accuracy of the acquired S-N curves for

both corroded and uncorroded specimens. Furthermore, the distribution and stand deviation of the specimens tested at $405MPa$ are less dispersed than those at $360MPa$, which is consistent with the fact that fatigue behavior of the same material would demonstrate more uncertainties and variations at relatively low stress levels than at higher stress levels.

Based on the acquired S-N curve data, cumulative damage behavior of the steel is tested at the same two stress levels, i.e., $360MPa$ and $405MPa$. 4 specimens are tested and categorized into two types: high-to-low and low-to high. In either case, the specimens would be subjected to the first loading level until it's 50% of estimated lifetime. Then specimens would be subjected to the second stress level until they fail. The acquired data is shown in Table 3.

Table 3 Cumulative damage of tested High-to-low and Low-to high samples.

Sample	Profile (MPa)	# of cycles 1	$\frac{n_1}{N_1}$	# of cycles 2	$\frac{n_2}{N_2}$	$\frac{n_1}{N_1}+\frac{n_2}{N_2}$
HL1	405-360	109818	0.50	102874	0.245	0.745
HL2	405-360	109820	0.50	101614	0.247	0.747
LH1	360-450	210738	0.50	104192	0.47	0.97
LH2	360-450	210748	0.50	166276	0.75	1.25

Cumulative damage curves of the tested two sets are shown in Figure 13. It's clearly seen that the cumulative damage behavior of tested specimens doesn't follow the Palmgren-Mine prediction, but instead has a non-linear damage cumulation.

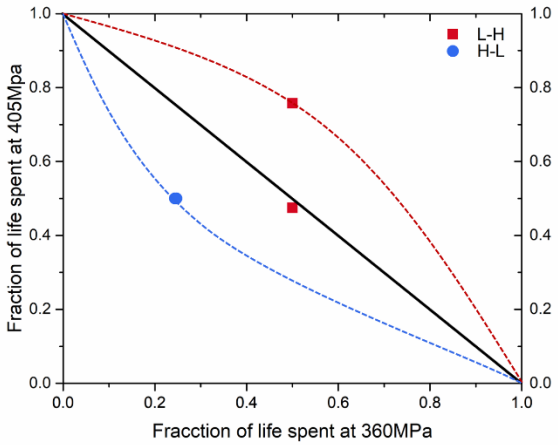

Figure 13 Non-linear cumulative damage of tested specimens.

2.4 Conclusions and Future Work

2.4.1 Conclusions

Morphological and quantitative analysis are carried out on the fatigue behavior of a certain type of steel by S-N approach, tested specimens are sorted into two categories by with/without corrosion surface, and the following conclusions can be drawn:

(1) Morphological study on the corrosion surfaces and fracture surfaces of the tested specimens by both scanning electron microscopy and optical profilometry shows the credibility of predicting crack nucleation sites when combined with the specimen geometry as well as loading conditions.

(2) Tested specimens demonstrate a typical S-N behavior showing the role that corrosion surfaces play in the overall fatigue lifetime. While the uncorroded specimens clearly show a S-N curve with a fatigue limit, specimens with corrosion surfaces have a shortened lifetime and a curve that doesn’t really possess a fatigue limit.

(3) The statistical analysis of the tested specimens at two constant amplitudes

showed relatively small statistical variations, which could stand as proof of the accuracy of the acquired S-N curves for both two types of specimens. Also, the statistical results is consistent with the fact that fatigue behavior of materials and components would demonstrate more and more variations when applied stresses are getting lower.`

2.4.2 Future work

(1) Information acquired by optical profilometry (such as surface roughness) can be valuable and helpful in investigating materials' fatigue properties. By utilizing such information, a quantitative model could be established to predict the crack nucleation site and overall lifetime at each stress level.

(2) More samples should be tested to acquire more data for a more accurate S-N profile of the tested material. Profiles with completely random amplitudes should also be applied.

Chapter 3

INVESTIGATION ON SUB-CYCLE FATIGUE CRACK GROWTH BEHAVIOR OF BRIDGE STEEL BY IN-SITU SEM TESTING

3.1 Introduction

Fracture mechanics has also been applied to help researchers understand the fundamental mechanisms of fatigue crack nucleation and propagation. Here, cyclic stress intensity factor is deemed as the essential parameter, and a variety of approaches have been proposed to correlate the fatigue crack growth with applied driving forces. Among all those copious approaches and theoretical models, Paris' law [2] has been widely adopted because of its capability of correlating the fatigue crack growth rate per cycle ($da\ /\ dN$) to the applied stress intensity factor range (ΔK) and predicting fatigue lifetime. A schematic illustration of different stages and mechanisms of fatigue crack nucleation and propagation, as well as the interpretation of Paris' law is shown in Figure 14.

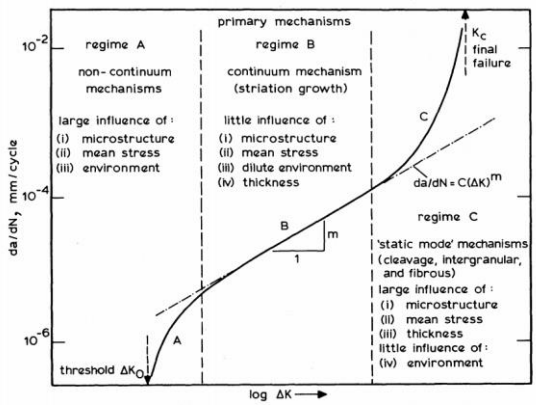

Figure 14 Schematic illustration of fatigue crack growth mechanisms and the Paris' law [12].

Numerous modifications on Paris' law have been proposed to improve the accuracy of the model by taking account into contributions from other parameters that

were not initially included by it. Among all these attempts to modify Paris' law, Elber's [13] is one of the most important because a brand-new phenomenon, defined as "crack closure", was incorporated into the fatigue crack growth model. During cyclic loadings, surfaces of a fatigue crack could contact each other and close even before the far-field stress reaches zero, and the crack would not reopen until a certain effective tensile stress is reached in the following cycle. The existence of crack closure phenomenon also suggests that one should apply an effective stress intensity factor range (ΔK_{eff}) instead of ΔK when studying fatigue crack behavior. Related studies on crack closure have been published by adopting theoretical and experimental methodologies [14]–[19]. Underlying mechanism of crack closure has been attributed to crack tip plasticity. A plastic zone is nucleated at the crack tip when cyclic stress is applied to the material, as the crack grows, a plastically deformed zone is produced at its wake, causing the crack surfaces to close before applied stress reaches to zero [20]. On the other hand, the existence and importance of crack closure have been remaining controversial for a long period of time, while some researchers strongly hold the opinion that crack closure serves a key role in fatigue crack growth [18], [21], [22], others oppose the importance of crack closure and argue that it only has trivial effect on overall fatigue crack growth [23]–[25].

Zizi Lu and Yongming Liu [3] proposed a new fatigue crack growth model at small time scales, Proposed methodology is fundamentally different from classical cycle-based fatigue models ($da\ /\ dN$) as it describes and predicts instant fatigue crack growth behavior ($da\ /\ dt$). Interaction of plastic zones ahead of crack tips are

considered, and crack closure is also regarded as an essential factor in fatigue crack growth. Two hypotheses are assumed when establishing the model: (1) Interactions between forward and reversed plastic zones play a dominant role in fatigue crack growth, and such growth behavior is affected by crack closure; (2) Crack growth demonstrates a non-uniform behavior within one loading cycle, that is, there would only be growth when the applied stress exceeds certain level during loading path, and there would be no growth during entire unloading path.

Two major obstacles that impede researchers from validating the proposed small-time-scale fatigue model are: (1) the necessity of high resolution microscopy. Average fatigue crack growth rates in Paris regime usually have the magnitudes of $10^{-8} - 10^{-5}\ m\ /\ cycle$, and measurements on such length scales are clearly beyond optical microscopies' capability; (2) usage of in-situ mechanical testing, which is critical for achieving real-time fatigue crack growth observations and measurements. With the assistance of high resolution scanning electron microscope (SEM) and in-situ mechanical testing, Wei Zhang [26] investigated the crack growth behavior of Al-7075-T6 alloys, with experimental study he verified the credibility of the above-mentioned model and hypotheses. By directly observations and image analysis, several pivotal conclusions have been drawn: (1) it has been confirmed that crack growth is not uniformly distributed through one cycle (i.e., no visible crack growth observed either during unloading paths or when stresses were lower than a critical level during loading paths), which proved the authenticity of the first hypothesis; (2) direct observation on crack closure phenomenon during in-situ SEM testing provided concrete proof of its

existence; (3) multiple mechanisms have been found co-existing within one cycle, and such co-existence leads to a nonlinear crack growth. Wei's predictions based on experimental procedures and observations showed decent match with regular CT specimen data from references, which indicates that the above-mentioned model can be trustfully extended to regular fatigue testing and analysis.

To simplify the crack closure calculation which is difficult because of the involvement of nonlinear analysis of cyclic plasticity and contact analysis, Wei [27] proposed a virtual crack annealing model to avoid above-mentioned complexities. He also proposed a model upon the crack opening stress calculation. Before his work, a model by Newman [21] is most widely adopted because of its capability of reducing computational costs. Proposed virtual crack annealing model was inspired by direct observations during in-situ SEM testing. Comparisons between Newman's model and Wei' model along with experimental validations can be seen in Figure 15. It can be concluded that Wei's model shows better agreement with experimental results at low stress ratios.

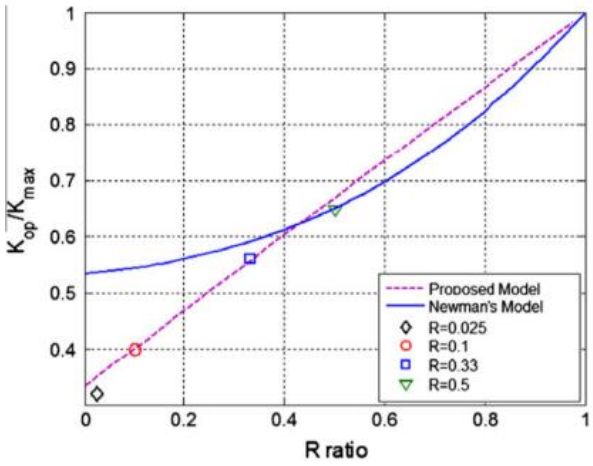

Figure 15 Comparison of experimental measured crack opening stress with model predictions [27].

3.2 Small-time-scale Crack Growth Model [3]

Above-mentioned small-time-scale crack growth model by Zizi Lu and Yongming Liu is reviewed in this section. Unlike classical fatigue crack growth models and theories, which are commonly cycle-based and correlate average crack growth rate per cycle ($da\ /\ dN$) with applied stress intensity factor range (ΔK), proposed small-time-scale crack growth model (schematically shown in Figure 16) lays its theoretical basis on instantaneous crack growth within one loading cycle ($da\ /\ dt$). Here, the continuous incremental in fatigue crack (da) within in one single cycle is defined as a function of change in applied stress ($dK\ /\ d\sigma$), and this concept is adopted as the key factor instead of the widely-used average crack growth rate ($da\ /\ dN$).

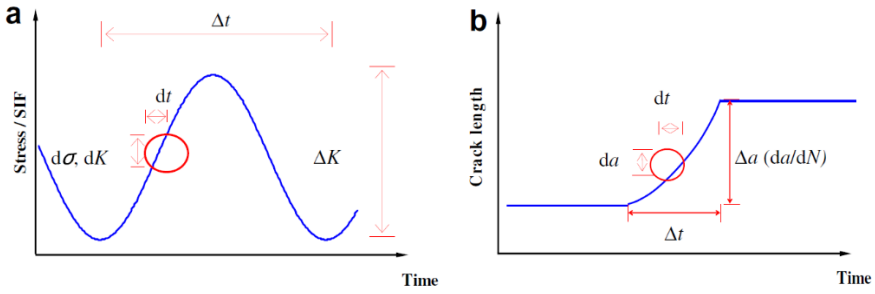

Figure 16 Schematic illustration of proposed model and its differences against classical cycle-based approaches: (a) stress/stress intensity factor (SIF) versus time; (b) crack growth versus time [3].

The instantaneous crack growth rate is calculated by the geometric relationship between crack tip opening displacement and crack growth (as is depicted in Figure 17), and is expressed as

$$da(t) = \frac{ctg\,\theta}{2} d\delta = C d\delta(t) \tag{2}$$

where $C = \frac{ctg\,\theta}{2}$, δ is CTOD, and θ is the crack tip opening angle (CTOA).

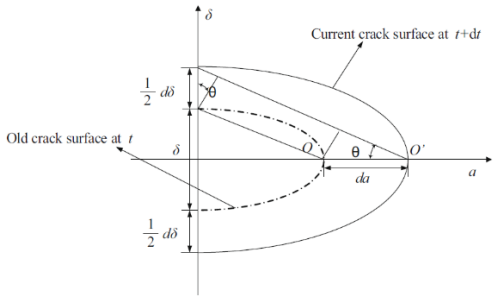

Figure 17 Schematic illustration of crack tip geometry [3].

Approximate expression of CTOD is shown as

$$\delta = \frac{K^2}{2E\sigma_y} \tag{3}$$

where E is Young's modulus, σ_y is yield strength of the material.

The instantaneous crack growth rate at arbitrary time is given by

$$\dot{a} = H(\dot{K}) \cdot H(K - K_{op}) \cdot \frac{CK}{E\sigma_y}\dot{K} \tag{4}$$

where H is Heaviside step function, K_{op} is the stress level at which crack opens and begins to grow. Total crack length at arbitrary time can then be calculated by taking integration of Equation 4 on both sides.

As discussed above, two hypotheses serve as prerequisites of the proposed small-time-scale fatigue model: (1) K_{op} is determined by the interaction between forward and reversed plastic zone, both of which are influenced by crack closure; (2) crack growth demonstrates a non-uniform behavior within one loading cycle. These hypotheses are incorporated into the model by the presence of Heaviside step function in the equation.

3.3 Experimental Setup and Procedures

3.3.1 Specimen Design and Preparation

Specimen geometry designed for the in-situ SEM testing is depicted in Figure

18. Machined and polished specimens are then precracked by MTS servohydraulic test system following ASTM E647-08: Standard Test Method for Measurement of Fatigue Crack Growth Rates. Specimens are installed into a pair of specifically designed grips to maintain the consistency of loading conditions, with a digital camera monitoring the precracking procedure, as is shown in Figure 19. All specimens are tested under constant loading amplitudes with loading ratios at $R = 0.1$, $R = 0.3$, and $R = 0.5$, respectively.

Considering the fact that critical parameters of the tested steel' mechanical properties are missing due to historical reason, they've been under service for quite long time, another set of specimens are prepared with Ti-6Al-4V, which is a type of widely used commercial titanium alloy in both commercial and military aircrafts. These titanium specimens are straightly fabricated out of a square plate, hence they would have the same thickness of $d = 1.5mm$ with the plate for the convenience of fabrication, the geometry of the fabricated specimens is shown in Figure 18. Mechanical properties of the Ti-6Al-4V alloy can be seen in Table 3.

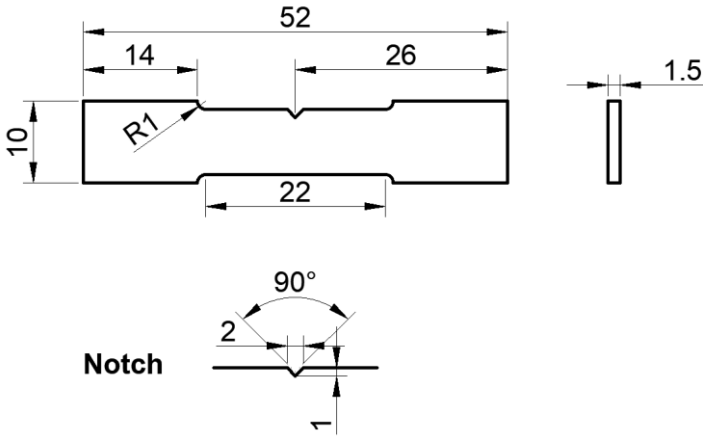

Figure 18 Geometry of the designed in-situ specimens.

Figure 19 Specimen precracking setup.

Table 4 Ti-6Al-4V mechanical properties.

Ultimate tensile strength	$900\sim950MPa$
Tensile yield strength	$880\sim920MPa$
Young's modulus	$104\sim113GPa$

Based on the geometry of the designed specimens and the loading conditions, specimens would be under plane stress condition during the in-situ SEM testing. It must be noticed that as the loading condition is defined as a single edge cracked geometry with clamped ends [28], [29], as is shown in Figure 20. A modified geometrical factor Y must be applied to the stress intensity factor equation $\Delta K = Y\Delta\sigma\sqrt{\pi a}$. Detailed derivations and numerical simulations on the geometrical factor can be found in the listed references.

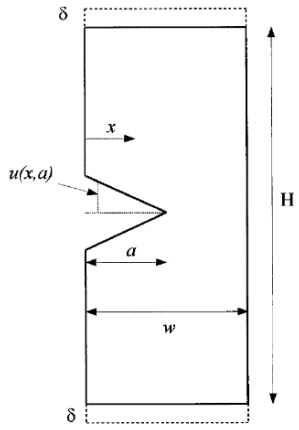

Figure 20 Illustration of the loading condition [29].

3.3.2 In-situ SEM Testing Setup

In-situ SEM fatigue testing plays a key role in validating the as-mentioned small-time-scale fatigue model. A tensile stage with load capacity of 1000lbs manufactured by MTI Instruments Inc. is installed into a ZEISS EVO MA 10 SEM, which enables the real-time tests and observations. The tensile stage is controlled by MTEST Quattro Materials Testing Software to enable its functionality by editing and running loading profiles. As-prepared specimens are installed into the mechanical grips, SEM and the in-situ SEM fatigue testing setup are shown in Figure 21.

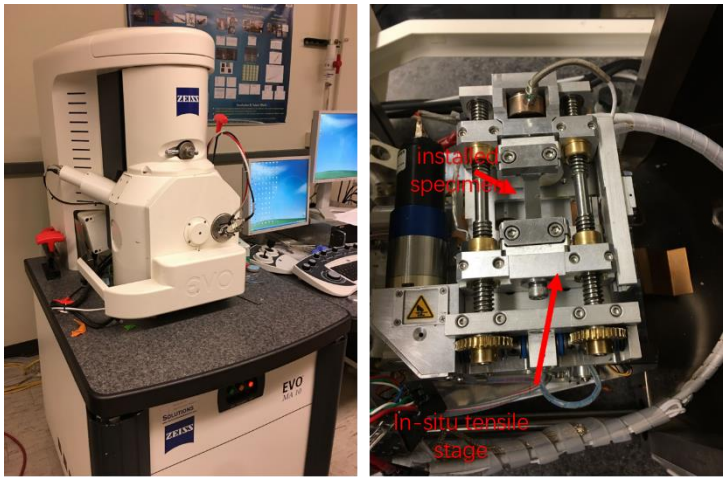

Figure 21 (a) ZEISS EVO MA 10 SEM; (b) in-situ SEM fatigue testing setup.

3.3.3 Experimental Procedures

Before starting the sub-cycle fatigue tests, a regular fatigue test with loading conditions consistent with precracking is implemented. This procedure is to make sure that the crack growth stabilizes. The crack is deemed as stable when the average crack growth rate has the magnitude of approximately $1\mu m\ /\ cycle$, which is commonly acknowledged as a decent rate that lies within the Paris region. Numbers of loading needed during this procedure vary because of the statistical variations of specimens.

During sub-cycle tests, one loading cycle is uniformly divided into different load steps, as is shown in Figure 22. Again, actual loading may vary due to the variances among specimens. The loading/unloading is controlled by the software above-mentioned with a relatively small rate of $0.03mm / s$ in displacement control. After each loading/unloading step is reached, the stage is suspended for the sake of observation and image capturing.

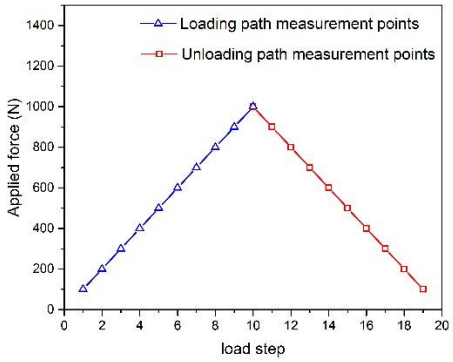

Figure 22 Schematic illustration of the measurement points during one loading cycle.

Images are captured at appropriate magnifications that could sufficiently contain all the necessary information. an object (dust particles, protrusions, etc.) far away from the vicinity of the crack but still lies within the same frame is intentionally used as a reference point to help maintain the crack positions in captured images, as is shown in Figure 23. By doing this, when combining all the images together and convert them into a GIF file, a smooth and continuous animation demonstrating the real-time fatigue crack growth can be obtained. It must be noticed that an image of the previous load peak is captured and saved as the reference peak, for the sake of measurements.

All gathered images are measured and analyzed by utilizing ImageJ image analysis software. Two critical parameters are carefully treated here: crack incremental

and CTOD. As is shown in Figure 23, measurements of these parameters are achieved by the following measuring procedures:

(1) An anchor point is manually selected (indicated by the yellow circle), which should normally be at the vicinity of the crack, or not far away from the edge in the image of reference peak.

(2) A horizontal reference line is drawn at the position of reference peak, which indicates the current horizontal position of the crack tip, as is shown by the black dash line. Then a normal to the horizontal reference line beginning at the anchor point is drawn, and its length is measured as the reference distance (length of the yellow dash line in Figure 23 (a) and (b)) for the first cycle (please be aware that the cycle from which image of the reference peak is captures should not be deemed as the first cycle). Since the first horizontal reference line go straight through the crack tip, the CTOD at this moment is 0.

(3) At each step of the first cycle, since the crack tip advances forward, the segment of the horizontal reference that goes across the crack is measured and deemed as the CTOD for each step, as is shown by the width of the red bracket in Figure 23 (b). This process is repeated for each load step of the entire cycle.

(4) The absolute distance of the line drawn between the anchor point and the crack tip at each load step is measured and denoted $a_n, (n = 1,2,3 \dots)$, hence the incremental crack length growth per load step is calculated by $\Delta a = (a_n - a_{n-1})$, as can be seen in Figure 23 (c) and (d).

(5) At the peak of the first cycle, a new anchor point can be set up (the same

anchor point can also be kept and used again, depending on which is more convenient), which will be used for the sake of measurements during next cycle. A new horizonal reference line is drawn at the new crack tip, which will be used to measure the CTODs during the next cycle.

(6) The whole process can be repeated to acquire data for a sequential of cycles.

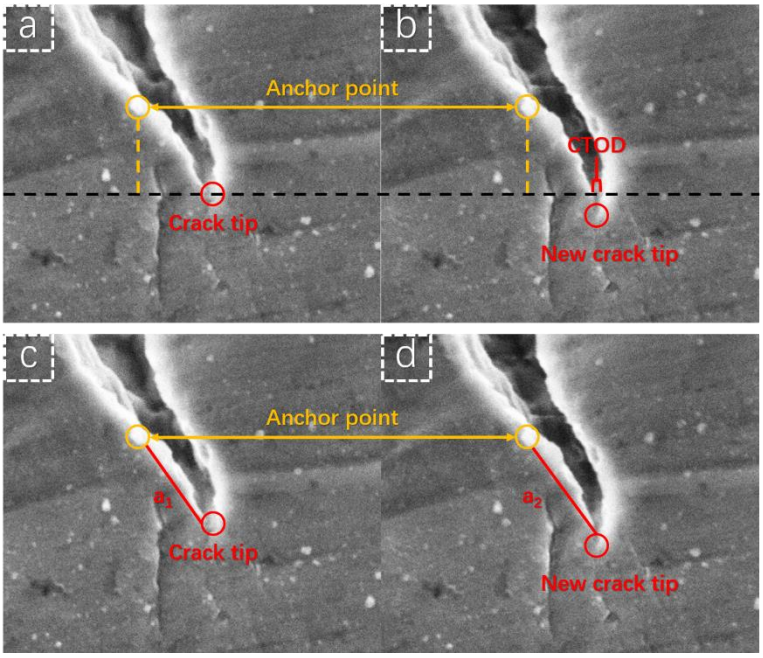

Figure 23 Measurements of CTODs and incremental crack growth a_n.

3.4 Results and Discussions

3.4.1 Morphological Analysis

An overall morphology with zoom-in features of the fatigue during the in-situ SEM fatigue tests is shown in Figure 24. The overall morphology indicates a transgranular crack growth behavior, which is consistent with classical theory on high cycle fatigue crack growth [30]. Detailed information can be obtained by TEM characterization and analysis.

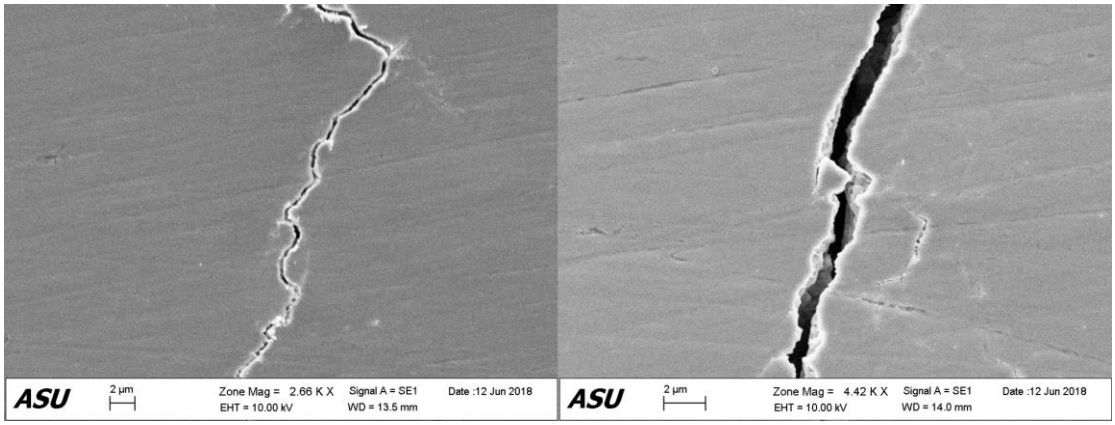

Figure 24 Overall morphology of the crack during the in-situ SEM fatigue test

A serial of selected images (for the reason of content length) illustrating images captured from loading path of 1 cycle of the tested specimen at ratio $R = 0.1$ is shown in Figure 25, and several qualitive conclusions can be drawn by direction observations. Incremental crack growth is accompanied by increments of CTODs during the loading path. Crack closure phenomenon is confirmed, as the crack remains closed in the Figure 25 (a) and (b), though stresses equivalent to 10 % and 30% of the maximum stress are applied to both load steps. Two surfaces of the closed crack show a serrate morphology because of the surface roughness. In Figure 25 (c), as the applied load continues to go up and exceeds a certain stress level, which is denoted as the crack opening stress, the crack starts to open, CTOD goes beyond zero and crack starts to grow.

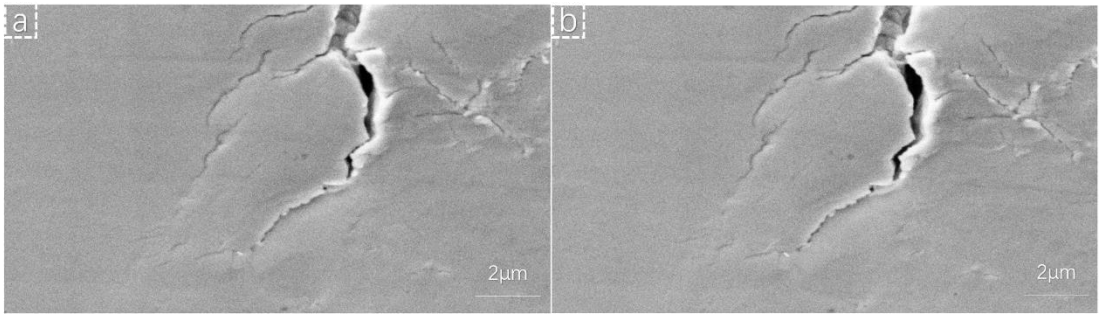

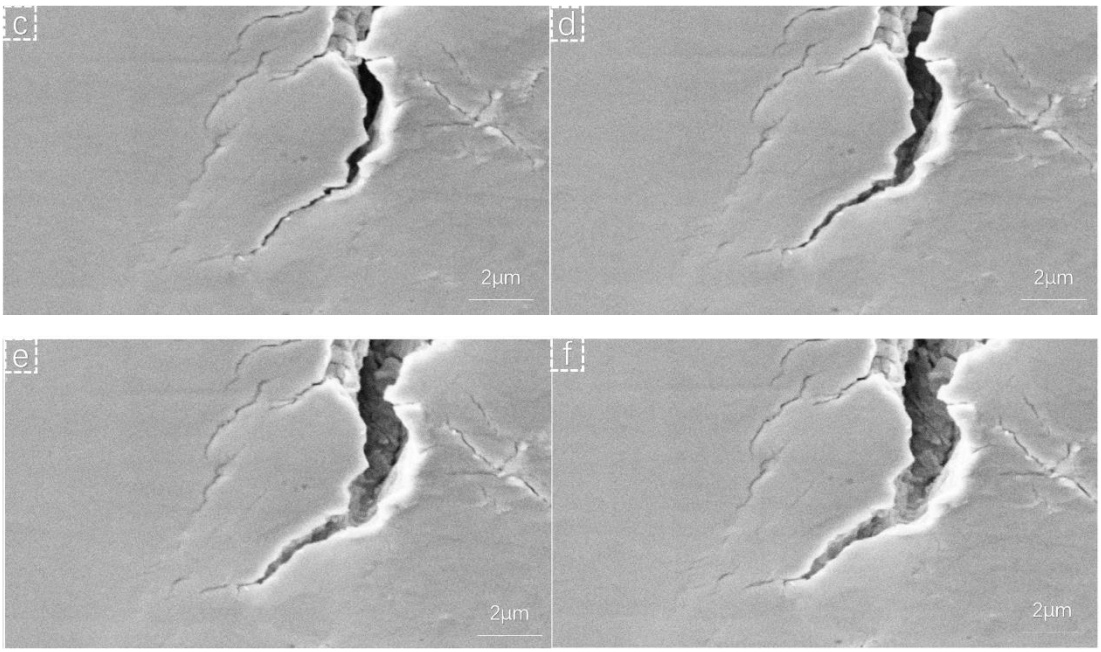

Figure 25 Images captured during the loading path of 1 cycle, (a)~(f) stand for 10%, 30%, 50%, 70%, 90% 100% of the maximum stress, respectively.

A micro-crack-oriented crack growth mechanism is observed. Figure 26 shows the fatigue crack of a titanium specimen subjected to of a constant loading with load ratio $R = 0.3$. Images are captured at loading peaks. Besides the main crack tip within in the red circle shown in Figure 26 (a), several micro cracks lie at the bottom right of the main crack are also detected. The red arrows indicate the predicted crack growth direction. Nevertheless, it can be seen that the for the next following cycles (Figure 26 (b), (c) and (d)), The crack deflected towards the micro cracks and gradually converge with the micro cracks into the new main crack. The existence of the micro cracks is explained by defects exist in commercial defects, which serve as local weaknesses and create stress concentration.

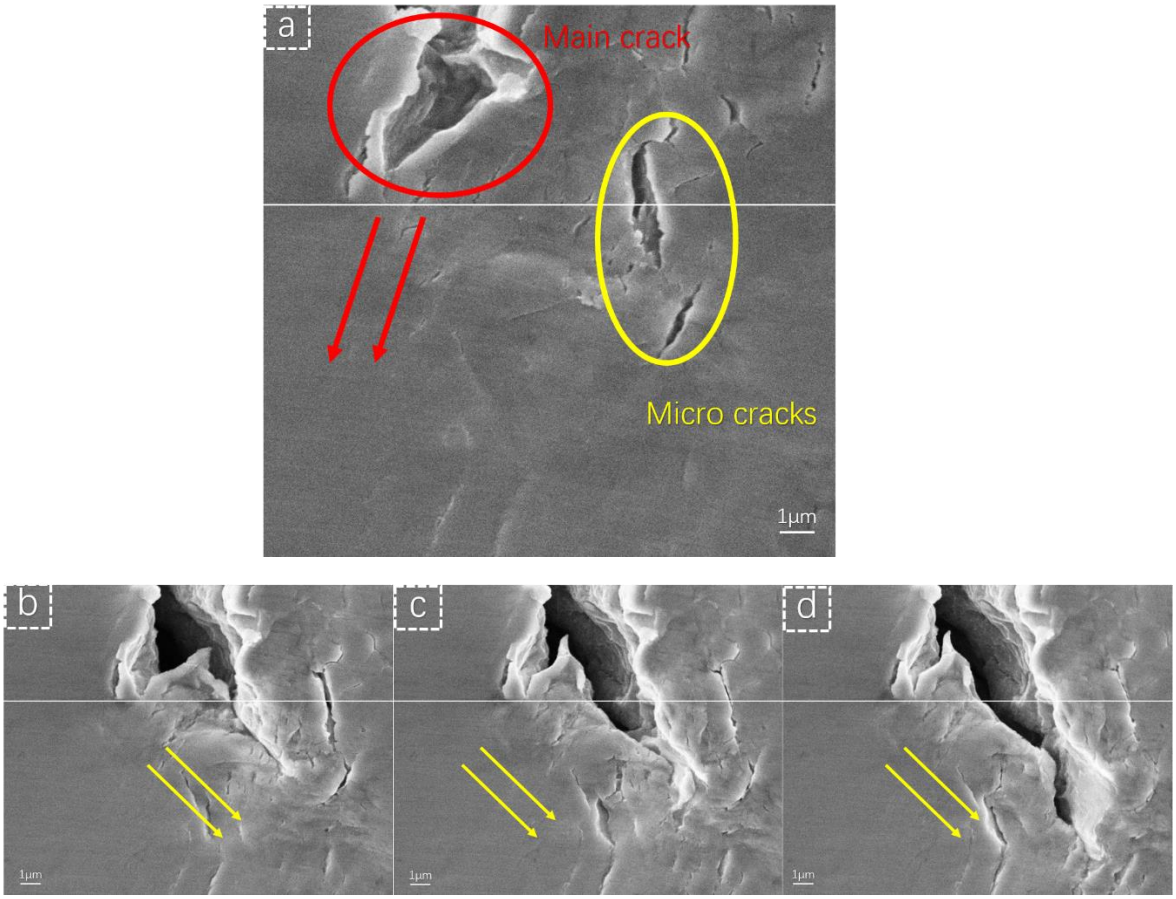

Figure 26 Micro-crack-oriented crack growth mechanism.

Tested bridge steel shows a stable crack closure phenomenon at small growth rates. Figure 27 illustrates the crack tip at minimum and maximum stress level within one loading cycle, with a $\Delta K = 20.85Mpa \cdot m^{0.5}$, The crack growth length within this loading cycle is measured to be $0.14\mu m$. Crack closure can be directly observed in these two images.

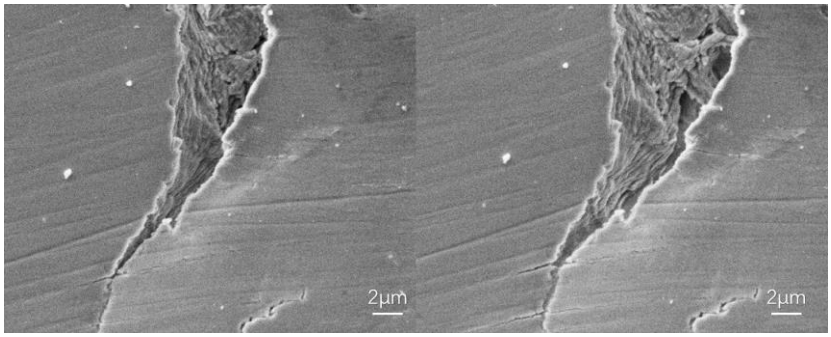

Figure 27 Crack tip at minimum and maximum stress level within one loading cycle.

When the applied stress goes beyond moderate levels but still theoretically lies within the Paris regime, the steel crack tips are observed to be severely blunted, and a riot morphology with branches around the main crack arises, as can be seen in Figure 28. Branches in Figure 28 (b) behave like intergranular cracks, which is characterized by low cycle fatigue with high local plasticity [30]. The reason that causes this remains unknown, and one possible explanation may lie upon the aging and natural degradation during the steel's decades of service.

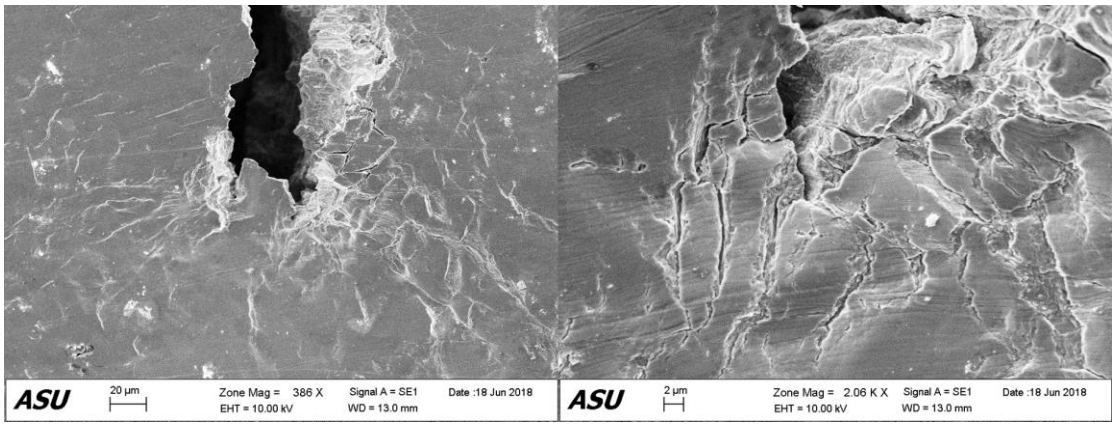

(a) (b)

Figure 28 Morphology of: (a) blunted crack tip; (b) zoom-in crack tip with branching.

3.4.2 Data Analysis

A CTOD versus SIF plot for a full loading cycle on Ti-6Al-4V is presented in Figure 29 (a), with $\Delta K = 21.69 Mpa \cdot m^{0.5}$ and stress ratio $R = 0.1$. Red arrows indicate both loading and unload paths. It can be directly seen that the measured CTODs remain 0 for the first few loading steps, providing a quantitative proof of the crack closure. As the applied stress exceeds certain level (which in this case is the crack opening stress), CTOD goes beyond 0 and starts to increase until the maximum stress is reached. During the loading and unloading path, even the applied stresses are the

same, the measured CTOD at each loading level are different, and clearly the CTODs during the unloading path are larger than those during the loading path. This is attributed to the retardation caused by forward and reversed plastic zones at crack tip. During the unloading path the crack closes at a stress level lower than the crack opening stress, such behavior is consistent with the theoretical predictions in [22]. Another plot with same principle from Wei's work [26] on aluminum alloy 7075-T6 is shown in Figure 29 (b). Both plots behave similarly and show all the above-discussed phenomena, hence validating the credibility of the proposed model [3], [26].

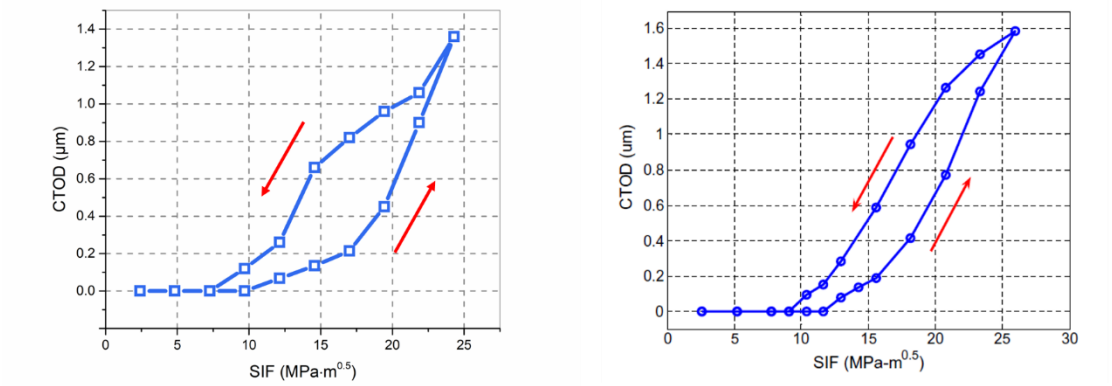

(a) (b)

Figure 29 CTOD versus SIF: (a) Ti-6Al-4V; (b) 7075-T6 [26].

The incremental crack growth per loading step Δa versus SIF of the same cycle is plotted depicted in Figure 30. The crack doesn't grow until the applied stress exceeds the crack opening stress level, and the growth clearly shows dependence with measured CTODs. The overall trend of the plot shows a non-uniform growth behavior during the loading path, which is identical with the model predictions. Both direct observations and measurements prove that the crack doesn't grow during the unloading path, indicating the validity of the second hypothesis.

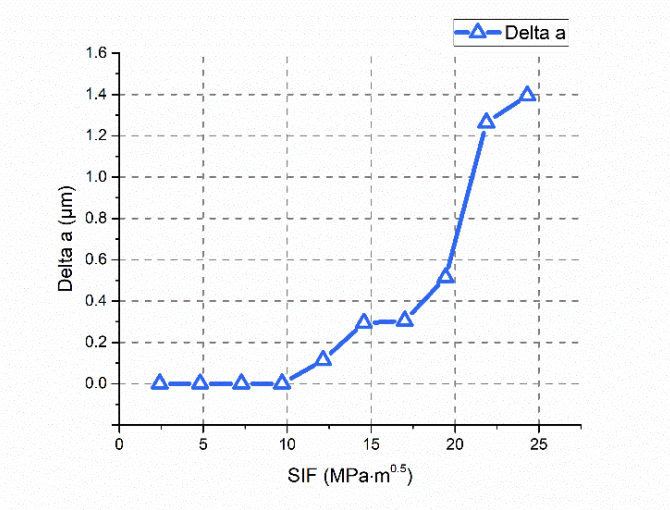

Figure 30 Incremental crack growth Δa versus SIF.

Figure 31 illustrates CTOD versus SIF during the loading paths for 4 consecutive cycles at $\Delta K = 25.29Mpa \cdot m^{0.5}$ and $R = 0.1$. At low stresses, the overall CTODs demonstrate crack closure behavior with a steady K_{op}. As the crack advances, the CTODs at maximum stress level during each cycle show increasements, indicating the interaction between incremental crack growth as well as the CTODs.

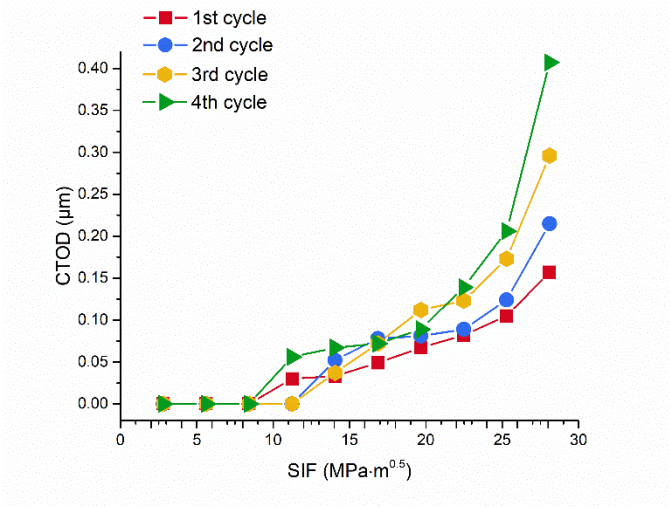

Figure 31 Incremental crack growth Δa versus SIF for 4 consecutive cycles.

For the same 4 consecutive cycles, Incremental crack growth Δa versus CTOD during the loading paths are plotted in Figure 32 (a). Though variations exist, the overall shape of the plots indicate a non-uniform crack growth behavior during loading paths.

Specifically, the growth behavior can be characterized by a bi-linear trend, as indicated by the light blue arrows. Such behavior was also experimentally validated in Wei's work [26], as is shown in Figure 32 (b). Region 1 indicates a brittle growth characterized with instantaneous crack growth rate identified by the slope, whereas region 2 stands for a blunting growth associated with large local plastic deformation.

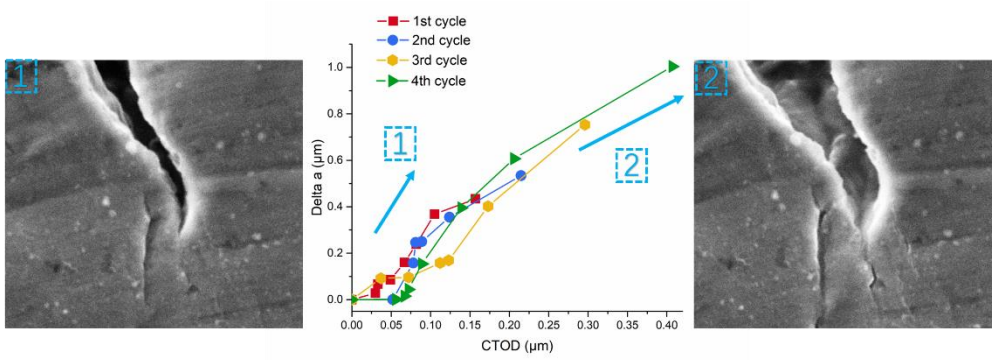

(a)

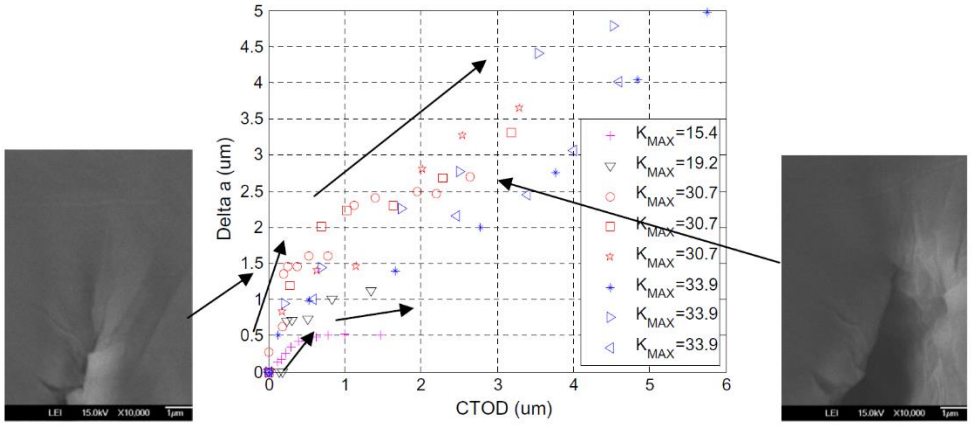

(b)

Figure 32 Incremental crack growth Δa versus CTODs during the loading paths.

Such bi-linear can be interpreted by following:

(1) In region 1, material in the very close front of the crack tip has already been weakened due to previous loading history and couldn't persist its original strength, though the crack tip has not advanced to its location and the surface remains morphologically intact. Hence during the next loading path, the crack advances

associated with a fast growth. The brittle growth comes from the compressive residual stress during previous loading history which would inhibit local plastic deformations. Hence, the overall growth behavior in region 1 would be a combination of fast and brittle growth along with little changes in CTODs.

(2) In region 2, as the applied stress goes up, effect of compressive residual stress has been outcome by large local plastic deformations at the crack tip, and the crack tip would behave a plastic growth manner. Local stress concentrations in two regions would be significantly different from each other due to their distinctive morphologies.

As three different loading ratios are applied during the tests, the accuracy of the proposed model on crack opening stress calculations by Wei [27] is also verified. The ratio between crack opening stress and maximum applied stress can be estimated by

$$\frac{\sigma_{op}}{\sigma_{max}} = 0.6R + 0.4 \tag{5}$$

where R is the loading ratios during the in-situ SEM tests.

Newman's model [21] for the plane stress scenario can be expressed by

$$\sigma_{op}/\sigma_{max} = 0.535 + 0.069R + 0.139R^2 + 0.257R^3 \tag{6}$$

Here the crack opening stresses are experimentally determined, and the results are plotted along with the two model predictions in Figure 33.

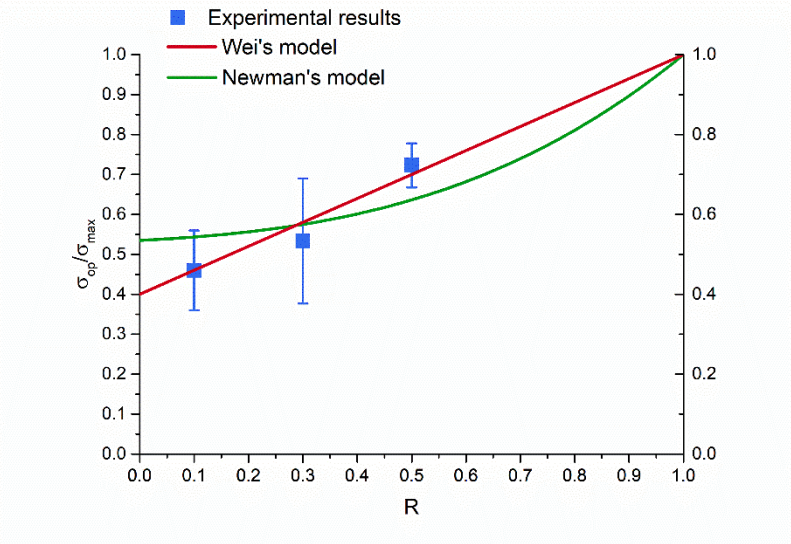

Figure 33 σ_{op} / σ_{max} versus loading ratios R.

Here blue squares stand for the experimental results with $R = 0.1$, $R = 0.3$, and $R = 0.5$, with error bars indicating variations. The red solid line stands for the model prediction by Wei's work [27], and the green solid line is calculated result by Newman's model [21]. Though variations do exist, the overall experimental results fit pretty well with predicted result from Wei's model, demonstrating the accuracy of the proposed model. Whereas for the Newman's model, experimental data doesn't show good fit at low ratios, and much larger values are predicted by Newman's model.

3.5 Conclusions and Future Work

3.5.1 Conclusions

Based on a small-time-scale fatigue model, in-situ SEM fatigue tests were run on both unknown bridge steel from Chapter 2 as well as Ti-6Al-4V, and both qualitive and quantitative conclusion can be drawn:

(1) By direct observations as well as measurements on CTODs during each loading cycles at variant loading ratios, crack closure phenomenon was confirmed in

both two different materials.

(2) Two fatigue crack growth behavior observed. The first one is the discontinuous fatigue crack growth model at very small crack growth grates. The second one is a micro-crack-oriented fatigue crack growth mechanism.

(3) A bi-linear crack growth behavior confirmed, and this is consistent with the experimental work on other materials by Wei [26]. Experimental results successfully validated the universality of the small-time-scale fatigue crack model.

(4) Experimental results show good fit with a crack tip opening stress proposed by Wei [27], indicating its accuracy.

3.5.2 Future Work

(1) More work should be done to explore the aberrant behavior of the bridge steel during in-situ SEM fatigue testing, as well as at Higher load ratios ($R = 0.7, R = 0.9$,etc.) for both materials.

(2) Explore the effects of single overload cycle/ underload cycle on the fatigue crack growth behavior by applying the small-time-scale model and in-situ SEM fatigue testing.

(3) More work could be done on extended materials, to help modify the proposed model and improve its accuracy.

REFERENCES

[1] S. Suresh, *Fatigue of Materials*. 1998.

[2] P. Paris and F. Erdogan, "A Critical Analysis of Crack Propagation Laws," *J. Basic Eng.*, vol. 85, no. 4, p. 528, 1963.

[3] Z. Lu and Y. Liu, "Small time scale fatigue crack growth analysis," *Int. J. Fatigue*, vol. 32, no. 8, pp. 1306–1321, 2010.

[4] A. International, "Fatigue," *Elem. Metall. Eng. Alloy.*, pp. 243–265, 2008.

[5] D. Project, I. N. Materials, and S. Cycle, "Corrosion-Fatigue Testing on Steel Grades With Different Heat and Surface Treatments Used in Rock-Drilling Applications," 2016.

[6] H. E. Boyer, "Atlas of Fatigue Curves," p. 518, 1985.

[7] ASM Handbook Comittee, *ASM Handbook, volume 13: Corrosion: Fundamentals, Testing, and Protection*. 2003.

[8] J. R. Donahue and J. T. Burns, "Effect of chloride concentration on the corrosion-fatigue crack behavior of an age-hardenable martensitic stainless steel," *Int. J. Fatigue*, vol. 91, pp. 79–99, 2016.

[9] J. R. Donahue, A. B. Lass, and J. T. Burns, "The interaction of corrosion fatigue and stress-corrosion cracking in a precipitation-hardened martensitic stainless steel," *npj Mater. Degrad.*, vol. 1, no. 1, p. 11, 2017.

[10] R. Ebara, "Corrosion fatigue crack initiation behavior of stainless steels," *Procedia Eng.*, vol. 2, no. 1, pp. 1297–1306, 2010.

[11] M. Suraratchai, J. Limido, C. Mabru, and R. Chieragatti, "Modelling the influence of machined surface roughness on the fatigue life of aluminium alloy," *Int. J. Fatigue*, vol. 30, no. 12, pp. 2119–2126, 2008.

[12] R. O. Ritchie, "Near-threshold fatigue-crack propagation in steels," *Int. Met. Rev.*, vol. 24, no. 1, pp. 205–230, 1979.

[13] ELBER W, "Fatigue Crack Closure Under Cyclic Tension," *Eng. Fract. Mech.*, vol. 2, no. 1, pp. 37–45, 1970.

[14] T. Chang, "Effects of strain hardening and stress state on fatigue crack closure," *Int. J. Fatigue*, 1999.

[15] S. Pommier and P. Bompard, “Bauschinger effect of alloys and plasticity-induced crack closure: A finite element analysis,” *Fatigue Fract. Eng. Mater. Struct.*, 2000.

[16] J. Zhang and P. Bowen, “On the finite element simulation of three-dimensional semi-circular fatigue crack growth and closure,” *Eng. Fract. Mech.*, 1998.

[17] J. Llorca and V. Sánchez Gálvez, “Modelling plasticity-induced fatigue crack closure,” *Eng. Fract. Mech.*, 1990.

[18] T. Chang and W. Guo, “A model for the through-thickness fatigue crack closure,” *Eng. Fract. Mech.*, vol. 64, no. 1, pp. 59–65, 1999.

[19] J. H. Kim and S. B. Lee, “Behavior of plasticity-induced crack closure and roughness-induced crack closure in aluminum alloy,” *Int. J. Fatigue*, 2001.

[20] C. k. k. meyers M.A., *Mechanical Behavior of Materials. 2007*. 2007.

[21] J. C. Newman, “A crack opening stress equation for fatigue crack growth,” *Int. J. Fract.*, 1984.

[22] B. Budiansky and J. W. Hutchinson, “Analysis of Closure in Fatigue Crack Growth,” *J. Appl. Mech.*, vol. 45, no. 2, p. 267, 1978.

[23] F. O. Riemelmoser and R. Pippan, “Crack closure: A concept of fatigue crack growth under examination,” *Fatigue Fract. Eng. Mater. Struct.*, vol. 20, no. 11, pp. 1529–1540, 1997.

[24] J. Z. Zhang, J. Z. Zhang, and Z. X. Meng, “Direct high resolution in situ SEM observations of very small fatigue crack growth in the ultra-fine grain aluminium alloy IN 9052,” *Scr. Mater.*, vol. 50, no. 6, pp. 825–828, 2004.

[25] A. Vasudevan, K. Sadananda, and N. Louat, “Reconsideration of Fatigue Crack Closure,” *Scr. Metall. Mater.*, vol. 27, pp. 1663–1678, 1992.

[26] W. Zhang and Y. Liu, “Investigation of incremental fatigue crack growth mechanisms using in situ SEM testing,” *Int. J. Fatigue*, vol. 42, pp. 14–23, 2012.

[27] W. Zhang and Y. Liu, “In situ SEM testing for crack closure investigation and virtual crack annealing model development,” *Int. J. Fatigue*, vol. 43, pp. 188–196, 2012.

[28] R. John and B. Rigling, “Effect of height to width ratio on k and cmod solutions for a single edge cracked geometry with clamped ends,” *Eng. Fract. Mech.*, vol. 60, no. 2, pp. 147–156, 1998.

[29] I. S. Jones, “A wide range weight function for a single edge cracked geometry with clamped ends,” *Int. J. Fract.*, vol. 89, no. 1, pp. 1–18, 1998.

[30] P. P. Milella, *Fatigue and corrosion in metals*. 2013.